Hybrid Simulations of the Effects of Interstellar Pick-up Hydrogen on the Solar Wind Termination Shock

P. C. Liewer
B. E. Goldstein
N. Omidi

CRPC-TR92282
October 1992

Center for Research on Parallel Computation
Rice University
P.O. Box 1892
Houston, TX 77251-1892

CRPC-92-2 October 19, 1992

Hybrid Simulations of the Effects of Interstellar Pick-up Hydrogen on the Solar Wind Termination Shock*

P. C. Liewer[1], B. E. Goldstein[1] and N. Omidi[2]

[1] *Jet Propulsion Laboratory*
California Institute of Technology
Pasadena, California 91125

[2] *Department of Electrical and Computer Engineering*
California Space Institute
University of California, San Diego
La Jolla, California 92093

* *This work was supported in part by the NSF under Cooperative Agreement No. CCR-8809615. The government has certain rights in this material.*

Hybrid Simulations of the Effects of Interstellar Pick-up Hydrogen on the Solar Wind Termination Shock

P. C. Liewer and B. E. Goldstein
Jet Propulsion Laboratory, California Institute of Technology, Pasadena

N. Omidi
Department of Electrical and Computer Engineering, California Space Institute, University of California, San Diego

Hybrid (kinetic ions/fluid electrons) plasma simulations are used to study the effects of a population of energetic interstellar pick-up hydrogen ions on the termination shock. The pick-up hydrogen is treated as a second ion species in the simulations and thus the effects of the pick-ups on the shock, as well as the effects of the shock on the pick-ups, are treated in a fully self-consistent manner. For quasi-perpendicular shocks with 10-20% pick-up hydrogen, the pick-up ions manifest themselves in a small foot ahead of the shock ramp caused by pick-up ion reflection. For oblique shocks with smaller angles between the field and the shock normal ($\theta_{Bn} \approx 40^o$-60^o), a large fraction of the pick-up ions are reflected and move back upstream where they excite large amplitude magnetosonic waves which steepen into shocklets. These backstreaming pickup ions may provide advance warning of a spacecraft encounter with the termination shock.

1. Introduction and Summary

The solar wind termination shock, expected to lie at 50-150 AU, will mark the transition of the solar wind flow from supersonic to subsonic flow in response to the pressure from the interstellar plasma. It has been suggested that this shock may differ from other shocks because of the relatively large fraction of the upstream energy carried by the interstellar pick-up ions. Pick-up ions result from interstellar neutrals which move unimpeded through the heliosphere at roughly the local interstellar flow speed (~20 km/sec) until ionized by UV radiation or collisions. Once ionized, the ions are moving relative to the solar wind with V_{SW}, the solar wind speed, and begin to gyrate in the magnetic field with gyro radius $\rho = V_{SW}\sin\theta/\omega_c$, where ω_c the pick-up ion gyro frequency and θ is the angle between the solar wind flow and the magnetic field. A ring distribution in velocity space is initially formed. Observations of pick-up He^+ from the AMPTE/IRM spacecraft

show that the pick-up ions have a spherically symmetric shell distribution in velocity space co-moving with the solar wind [*Mobius et al.*, 1985]. This distribution results from rapid pitch angle scattering of the pick-up ions in background and self-generated MHD fluctuations in the solar wind [*Mobius*, 1986; *Mobius et al.*, 1988]. Energy diffusion is unimportant for these ions, and the distribution is not observed to thermalize [*Mobius*, 1986; *Mobius et al.*, 1988]. The observed partial filling of the spherical shell distribution results from adiabatic cooling of the pick-up ions as the solar wind expands [*Mobius et al.*, 1988].

Pick-up hydrogen is expected to be the dominant pick-up species because interstellar neutral hydrogen has a much higher density than other interstellar neutrals and it is more easily ionized [*Mobius*, 1986]. The percentage of H^+ to solar wind ions at 50 AU is estimated to be 10% and increases linearly with distance from the sun [*Vasyliunas and Siscoe*, 1976; *Lee*, 1987]. The first observations of pick-up hydrogen have recently been made using the SWICS instrument on board the Ulysses spacecraft by *Gloekler et al.* [1992] who found the density of neutral hydrogen at 5 AU was about a factor of 5 lower than standard model predictions. These measurements indicate that the H^+ pick-up ions undergo rapid pitch angle scattering, but little energy diffusion. Dynamics of pick-up ions at the termination shock are of interest not only because of their possible effect on shock structure, but also because it has been hypothesized that these ions may form the seed population for the anomalous component of cosmic rays [*Fisk et al.*, 1974; *Fisk*, 1986; *Pesses et al.*, 1981;*Jokipii*, 1986, 1992;].

The effects of heavy pick-up ions on cometary shocks have been studied by *Omidi et al.* [1986] and *Omidi and Winske* [1987, 1991] using one-dimensional hybrid simulations. *Omidi et al.* [1986] studied the effects of pick-up O^+ ions of various assumed velocity distributions on supercritical quasi-perpendicular shocks and found that when the O^+ ions were assumed to have a ring-beam velocity distribution, an extended foot was seen on the shock due to the reflection of O^+ ions from the shock front. In *Omidi et al.* [1986], a hard piston was used to drive the shock. To include the effects of mass loading on cometary shock formation, *Omidi and Winske* [1987,1991] performed simulations with O^+ ions created throughout the simulation volume. No hard piston was used, but rather the shock formed as a result of mass loading. Due to computational limitations, only a small portion of the true solar wind-comet interaction region was modeled [*Omidi and Winske*, 1987, 1991]. For cometary shocks, ion pick-up and pitch-angle scattering processes, as well as solar wind mass loading and deceleration, all occur where the shock is forming.

In contrast to cometary shocks, for the termination shock, the interstellar ion pick-up, pitch angle scattering and mass loading processes occur not where the shock is

forming, but throughout the heliosphere. The interstellar pick-up H^+ iones are created at a rate scaling approximately as r^{-2}[*Mobius et al.*, 1988 and references therein]. Since the solar wind density also falls of as r^{-2}, the relative pick-up ion density and the mass loading increase approximately linearly with distance from the sun, with mass loading estimated to be about a 10% effect at 50 AU [*Holzer*, 1972; *Lee*, 1987]. Pitch angle scattering processes isotropize the pick-up ion distribution in velocity on a fraction of an AU scale [*Mobius et al.*, 1988]. Thus, in studying the effects of pick-up ions on the termination shock, one can assume that the pick-up, mass loading, and pitch angle scattering processes are for the most part complete before the solar wind reaches the termination shock.

Here, we present results from one-dimensional hybrid (particle ion/fluid electron) simulations of the termination shock with a population of interstellar H^+ pick-up ions. The pick-up ions are treated as a second species in the hybrid code and thus the effects of these ions on the shock and the effects of the shock on the ions are include in a fully self-consistent manner. The pick-up ion velocity distribution is assumed to be a spherical shell co-moving with the solar wind with radius V_{sw} [*Mobius et al.*, 1988]. For simplicity, we assumed a zero-thickness shell, thus neglecting the effects of the adiabatic cooling. The location of the termination shock and the fraction of pick-up hydrogen at the termination shock are unknown. We assume a termination shock location of about 50-100 AU and use 10-20% H^+ pick-ups, based on model predictions [*Lee*, 1987 and references therein]. Because of their higher energy, the interstellar pick-up ion $\beta_p >> 1 > \beta_i$ (where β_i is the beta of the thermal solar wind ions) even at 10% pick-up hydrogen density. The simulations were performed on the Intel Delta Touchstone parallel supercomputer at Caltech.

We find that for high Mach number quasi-perpendicular shocks ($\theta_{Bn} = 80^o$), reflection of the interstellar pick-ups at the shock ramp leads to the formation of a foot which scales with the pick-up ion gyroradius. The reflected pick-ups then turn and re-enter the shock, gaining some energy in the process. Because of their initial high energy, the relative temperature increase due to the shock crossing is not much more than adiabatic. The thermal solar wind ions provide most of the dissipation for the shock, and, in turn, are "heated" much more than adiabatically. However, as the fraction of pick-up hydrogen is increased from 10% to 20%, significantly more dissipation is caused by the pick-up ions. For oblique shocks with smaller angles between the field and the shock normal ($\theta_{Bn} = 40^o$–60^o), a large fraction of the pick-up ions are reflected back upstream, gaining energy in the process. Large amplitude magnetosonic waves excited by the reflected pick-up ions are observed in the simulations. The waves are swept back into the shock, steepening in the process.

The organization of this paper is as follows. The simulation model and the choice of parameters for the termination shock simulations are discussed in Section 2, the simulation results for quasi-perpendicular and oblique shocks are described in Section 3, and the results are discussed in Section 4.

2. Simulation Model and Termination Shock Parameters

2.1 Description of the Model

A one-dimensional hybrid plasma particle simulation code with particle ions and massless fluid electrons was used for these studies. This code is similar to that described in *Winske and Leroy* [1985] and *Leroy et al.* [1982]. Ions are treated as particles moving in (x,v_x,v_y,v_z) phase space under the influence of the Lorentz force; electrons are treated as a massless, charge neutralizing fluid. Fluid variables are treated as functions of time and one spatial dimension (x--the direction along the shock normal). In the version used here, the position and velocity of both thermal and pick-up ions are advanced one time step using a leap-frog scheme. The fluid moments (density and velocity) are next computed by interpolation of the particle information to the grid. Quasi-neutrality is assumed so that the electron density is found from the ion densities and the electron velocity in the x direction (the direction of variation) from the ion x-velocities. An implicit matrix equation is solved for the magnetic vector potential at the new time [*Winske and Leroy*, 1985]; the y and z electric and magnetic fields are next found from the vector potential. The total y and z currents are obtained from the curl of the magnetic field and the electron v_y and v_z are determined from the total current and the ion current. The electrons are assumed to heat adiabatically with $\gamma = 5/3$. Lastly, the x electric field is determined from the electron x-momentum equation in the massless electron limit.

For the studies here, the code was modified to include a second ion species, the interstellar pick-up ions, which are initialized with a spherical shell distribution in velocity space as opposed to the maxwellian distribution of the thermal solar wind ions. For simplicity, we assume a spherical shell velocity space with zero width and a radius equal to the solar wind velocity co-moving with the solar wind ions.

To generate a shock, the ions are injected from the left end of the simulation box and reflect off the right wall (the piston). The downstream velocity is then zero and the simulation is done in the downstream frame. To set boundary conditions for a particular shock, the Alfvenic Mach number and the plasma β are specified as input and the jump in the magnetic field and velocity for this shock are computed. The ion injection velocity u_x is

then computed in the downstream frame and used to initialize the ions. For the field equations, the magnetic field is specified at the right hand boundary and the convective electric field $E_y = u_x B_z$ at the left hand boundary. The shock forms at the right hand wall and propagates to the left with $v_{shock} \approx M_F V_F - u_x$ where the subscript F refers to fast magnetosonic mode. Note that the jump in the magnetic field and velocity across the shock are computed assuming a purely thermal ion distribution, and thus the actual Mach number and shock speed will be different for simulation with two species of ions with different temperatures.

The code uses dimensionless units with length normalized to c/ω_{pi} where ω_{pi} is the ion plasma frequency ($\omega_{pi}^2 = 4\pi n^0 e^2/m_p$ with m_p the proton mass, n^0 the initial total density, and e the proton charge), velocities are normalized to c, and time to ω_{pi}^{-1}. In the figures, the time has been normalized to ω_{ci}^{-1}. Typical runs had a time step of $0.025\omega_{ci}^{-1}$, a system length of 250-500 c/ω_{pi} with 2000-4000 grid points and ran for 1500-3000 time steps. For solar wind parameters at about 80 AU, the time step corresponds to about 6 secs and $c/\omega_{pi} \approx 7000$ km.

The computation were performed using 8-16 processors of the 512 processor Intel Delta Touchstone Parallel computer at Caltech. The computation was divided among the processors by dividing the particle computation only equally among the processors and using global communication on the field arrays; this is the simple decomposition described in *Liewer and Decyk* [1989]. The field solve was done sequentially in each processor. A typical run time was 30-60 minutes for a computation with 200,000 particles, 2000 grid points run for 2000 time steps.

2.2 Termination Shock Parameters

The plasma parameters at the termination shock, as well as its location, are unknown and thus the parameters used for the simulations are extrapolations from existing data. Five dimensionless parameters are needed to specify the shock simulations: the fractional density of the interstellar pick-up hydrogen, the Mach number of the shock, the electron and ion β ($\beta = 8\pi nT/B^2$), and ω_{pi}/ω_{ci} where $\omega_{ci} = eB_0/m_p c$ with B_0 is the solar wind field strength. In addition, the angle between the shock normal and the magnetic field θ_{Bn} must be set. The density, magnetic field and velocity of the solar wind are, of course highly variable, both at 1 AU and in the outer heliosphere (as measured by the Pioneer and Voyager spacecraft at 30-50 AU) and thus we chose representative values. No significant decrease in the solar wind speed has as yet been measured by any of the Pioneer or Voyager spacecraft and thus we have assumed that the solar wind speed at the termination

shock is comparable to that at earth. In the outer heliosphere, the magnetic field is dominated by the azimuthal field except near the poles so $B_0 \propto r^{-1}$ where r is the distance from the sun. The plasma density scales as r^{-2} and thus both the Alfven speed and the ratio ω_{pi}/ω_{ci} are independent of r. Since both the solar wind speed and the Alfven velocity are independent of r, the Mach number of the termination shock will be comparable to the Mach number at earth. Using for values at 1 AU a magnetic field of approximately 5-6 nT (and assuming the azimuthal field is 0.7 of this), a plasma density of 6 cm^{-3} and a solar wind velocity of 250-400 km/sec, we obtain $M_A \approx 5$-8 and $\omega_{pi}/\omega_{ci} \approx 7000$. This range of Mach numbers also allows for the possible reduction in the solar wind speed due to mass loading by interstellar pick-ups, which is estimated to be a 10% effect at 50 AU [*Holzer*, 1972].

Although the termination shock will on the average be perpendicular, the measured distributions of the azimuthal angle of the interplanetary magnetic field and the solar wind flow in the outer heliosphere are quite broad [*Smith*, 1990]. Shown in Figure 1 is a histogram of the azimuthal angle of the magnetic field at 35 AU obtained from hourly averaged Pioneer 11 magnetic field data [*Smith*, 1992]. The distributions are centered on the Parker angle (90° and 270°, depending on the sector), but have a broad distribution with a half width of about 25°. At this time (1991), Pioneer 11 was about 15° out of the ecliptic. Thus near the ecliptic, the angle between the field and the flow will frequently be less than 60°. Moreover, the shock becomes more parallel towards the poles of the heliosphere. Thus we have run cases for a variety of angles, θ_{Bn} =40°-80°. Note that we have been able to specify the shock Mach number, the angle θ_{Bn} and ω_{pi}/ω_{ci} without specifying the distance to the termination shock. The only remaining parameters are the density of pick-up hydrogen and the electron and ion $\beta = 8\pi\, nT/B_0^2$ in the outer heliosphere. The ratio n/B_0^2 is independent of distance, but it is necessary to make assumptions about the variation in the temperatures with distance. The plasma cools from expansion but heats from stream-stream interactions as well as by wave-particles interactions including instabilities excited by the interstellar pick-up process. Although very little is known about the temperature variation in the outer heliosphere, it is expected that the β's will be significantly lower than the values of $\beta \sim 1$ at 1 AU and, for $\beta < 1$, results are generally insensitive to the exact value. Pioneer data indicates that $\gamma_i \approx 1.1$–1.2 where $T \propto r^{-2(\gamma-1)}$. At 1 AU, $T_e \approx 16$ eV ($\beta_e \approx 1.1$) and $T_i \approx 6$ eV ($\beta_i \approx 0.4$). Taking $\gamma \approx 1.1$, we find $\beta_e \approx 0.5$ and $\beta_i \approx 0.2$ at ~80 AU. We have also run simulations with $\beta_e = \beta_i = 0.1$ to test the sensitivity of the results to the choice of β.

3. Simulation Results

3.1 Quasi-Perpendicular Shocks (θ_{Bn}= 80°)

Because of the tightness of the Parker spiral in the outer heliosphere away from the poles, the termination shock is expected, on the average, to be nearly perpendicular. Thus, simulations are first presented for nearly perpendicular shocks with θ_{Bn}= 80°. The first case, Case 1, is for a simulation with 10% pick-up hydrogen, M_A = 8, ω_{pi}/ω_{ci}= c/V_A=7000, β_i= 0.2, β_e= 0.5 and a phenomenological resistivity $\eta/4\pi$=2 x $10^{-5}/\omega_{pi}$ which corresponds to an anomalous collision frequency of about $0.08\omega_{pi}$. Figure 2 shows results from this simulation at a time $t\omega_{ci}$ = 60 plotted as a function of x (normalized to c/ω_{pi}). Plotted in Figure 2a as a function of x are the total magnetic field $B/B_0 = (B_x^2 + B_y^2 + B_z^2)^{-1/2}/B_0$ where B_0 is the initial magnetic field (note that B_x is constant throughout); the total plasma density $n/n^0 = (n_{sw} + n_p)/n^0$, where n^0 is the initial value; the solar wind(n_{sw}/n^0_{sw}) and pick-up ion (n_p/n^0_p) densities normalized to their upstream values; and the solar wind($4\pi n^0 T_{sw}/B_0^2$) and pick-up ion ($4\pi n^0 T_p/B_0^2$) temperatures. Using this normalization for the temperatures, the local β of species α can be obtained from $\beta_\alpha = 2\,(n_\alpha/n^0_\alpha)\,(n^0_\alpha/n^0)\,(4\pi n^0 T_{sw}/B_0^2)/(B/B_0)^2$. The temperature computed is the total temperature calculated from the particles velocities, *e.g.*, $T = \frac{1}{3} m \sum (\bar{v}^2 - \langle \bar{v}^2 \rangle)$. Plotted in Figure 2b are the solar wind (labeled S-W Ions) and H^+ pick-up ions (labeled Hpickup) phase space with the velocities normalized to c. The same normalizations are used in all of the figures. Note the change of scale for the velocity between the solar wind and pick-up ions. Although the pick-up ions represent only 10% of the density, because of their high energy, the pick-up $\beta_p \approx 5$ versus a solar wind ion $\beta_{sw} \approx 0.2$. However, upstream of the shock, the momentum flux is dominated by the solar wind flux, with $\rho V_{up}^2 > n_p T_p > B^2/8\pi >> n_{sw} T_{sw}$ where ρ is the total solar wind mass density.

Note in the magnetic field profile in Figure 2a that a foot extends ahead of the magnetic ramp. Comparison with the plot of the pick-up ion density in Figure 2a and the phase space plot in Figure 2b shows that it is the pick-up ions which are responsible for this foot. Apparently backstreaming pick-up ions are causing the observed foot in the magnetic field and the total density. The foot extends about 6 c/ω_{pi} ahead of the shock which is comparable to the gyroradius of the interstellar pick-up ions of approximately $8c/\omega_{pi}$. These backstreaming ions are then turned by the magnetic field and pass back through the shock front. These backstreaming ions may be ions which were reflected off the shock front or they may be ions which leaked through from behind the ramp.

Inspection of the solar wind phase space plot in Figure 2b shows a bi-modal distribution indicating that some solar wind ions have probably reflected from the shock front. After gaining energy via the reflection process, these ions are turned by the magnetic field and pass back through the ramp, forming a gyrating beam with a gyration velocity comparable to the upstream velocity. The phase space plots show the type of reflected -- gyrating beam seen in simulations of supercritical shocks [*Leroy et al.*, 1982; *Winske and Leroy*, 1985]. The very large in-phase oscillations in B and density immediately behind the shock front result from this gyrating beam; the plot of the solar wind fluid velocity (not shown) has the corresponding large oscillation 180° out of phase with those of n and B.

For this shock, the magnetic field and the solar wind and pick-up ion densities and the magnetic field jump by about a factor of 3 across the shock and the x velocity decrease by about 3 (in the shock frame). The temperature of the pick-up ions increased by about a factor of 3 which is the increase expected from adiabatic compression ($\gamma = 2$). Behind the shock, the solar wind momentum flux and the pressure in the pick-up ions are comparable to each other and greater than the magnetic and solar wind pressures.

The solar wind ions are 90% of the total density and provide most of the dissipation for the shock. The bi-modal distribution function of the solar wind ions gives rise to the large "temperature" increase plotted in Figure 2a, indicating that solar wind temperature has increased by about a factor of 20 across the shock. The ratio of the upstream velocity, and thus the gyration velocity, to the initial thermal velocity is $M_A V_A/v_{th,i} = M_A(2/\beta_i)^{1/2} \approx$ 25, and thus the ions in this reflected-gyrating beam contribute heavily to the computed temperature since $T \propto v^2$. Note that the phase space shows that the ions have not yet thermalized, even well behind the shock front, so the temperature plotted may not represent the true downstream temperature. No clear reflected gyrating beam is visible in the pick-up ion phase space, but since the initial thermal velocity of the pick-up ions is approximately the downstream velocity, it would be difficult to distinguish the gyrating beam pick-up ions from the others.

To study the effects of increasing pick-up ions density, a case with the parameters of Case 1, but with 20% hydrogen ions was run (Case 2, Figure 3). Plotted in Figure 3a as a function of x at $t\omega_{ci} = 60$ are the total magnetic field; total, solar wind and pick-up ion densities; and solar wind and pick-up ions temperatures, all normalized as in Figure 2. Plotted in Figure 3b are the solar wind and pick-up hydrogen phase spaces with velocities normalized to c. Again, note the change in scale of the velocities between the solar wind and pick-up ion phase space plots. Note that the extended foot on the magnetic ramp, caused the pick-up ions, is larger in this case, as expected. The shock propagates

somewhat faster in this case due to the increase in the upstream magnetosonic speed resulting from the increased "hot" pick-up component.

As in Case 1, the jump in the densities and the magnetic field is about a factor of 3 with a corresponding decrease in the x-velocities of about 3. Again, a gyrating beam is clearly visible in the solar wind ion phase space; comparison of this phase space with the Case 1 phase space in Figure 2 suggests that here a smaller fraction of the downstream ions are in the reflected-gyrating beam. This is supported by a smaller jump in the apparent solar wind ion temperature (a jump of a factor of 13 in Case 2 compared to a jump of 20 in Case 1). Thus apparently the solar wind ions are providing less of the shock dissipation in this case. The pick-up ion v_y-x phase space in Figure 3b shows some hint of a gyrating--reflected beam population. This is supported by the observed oscillation in the pick-up ion density (Figure 3a) and a corresponding out-of-phase oscillation in the pick-up ion downstream velocity (not shown). In this case, the pick-up ion pressure dominates the downstream moment flux, e.g., the downstream pick-up ion pressure is greater than the downstream solar wind moment flux and magnetic pressure.

To investigate the sensitivity of the results to resistivity, a case (Case 3, not shown) was run with the same parameters of Case 1, but with no resistivity, $\eta = 0$. Again an extended foot was seen ahead of the main shock ramp coincident with the increase in the pick-up ion density. The main difference between the case with no resistivity and Case 1 was the observations of large oscillations in B and density well behind the shock front. Immediately behind the shock, the oscillations are due to the gyration of the reflected solar wind ions passing back through the shock as is evidenced by the anti-correlated fluctuations in density and x velocity [*Leroy et al.*, 1982]. Further behind the shock the oscillations were identified as a mirror mode instability because 1) the fluctuations in density and B were anti-correlated, 2) there were no corresponding fluctuations in v_x, 3) the modes were non-propagating as seen from animation of magnetic field plots. The mirror mode was most likely driven by the large temperature anisotropy caused by the gyrating beam. The temperature anisotropy appears comparable in Cases 1 and 3, suggesting that the resistivity has damped the mode in Case 1.

3.2 Oblique Shocks (θ_{Bn}= 40°–60°)

Although the termination shock is expected to be close to perpendicular on the average, the measured angle between the solar wind magnetic field and the flow at 35 AU (Figure 1) shows that the angle fluctuates appreciably in the outer heliosphere and thus the

shock angle will frequently be in the range θ_{Bn}= 40°–60°. For such angles, it is well known that reflected ions can escape back upstream.

Figure 4 (Case 4) shows results from a simulation with θ_{Bn}= 50° and M_A = 5, with the other parameters as in Case 3 (no resistivity, 10% pick-up hydrogen) at $t\omega_{ci}$ = 80. Plotted in Figure 4a are the y and z components of the magnetic field, B_y/B_0 and B_z/B_0; the phase angle ϕ (in degrees) between B_y and B_z ($\tan\phi = B_z/B_y$); and the total, solar wind, and pick-up ion densities, normalized as in Figure 1. In Figure 4b, the solar wind and pick-up ion phase spaces are shown. A noticeable fraction of the pick-up ions can be seen moving back up stream (ions with negative v_x); no solar wind ions are visible upstream. A large amplitude wave (with $\delta B_y/B_0 \approx 25\%$) is evident in front of the shock. These waves are identified as compressive magnetosonic waves because of the correlation between the density and magnetic field fluctuations and because of the apparent steepening of the waves. The phase angle plots indicates that these waves are elliptically polarized. These large amplitude magnetosonic waves, which propagate upstream in the solar wind frame, have evidently been excited by the pick-up ions which have been preferentially reflected by (or leaked from) the shock and moved back upstream; these upstream pick-up ions are more easily seen in computer animation of the phase space plots. Simple calculations of ion mirroring in the de Hoffman-Teller frame were made to calculated the fraction of a shell distribution which would be reflected by a jump in B of the approximate size in the simulations. These calculations, which assumed that the ions remained adiabatic, indicate that for θ_{Bn}<60°, a large of the ions are reflected (66% for θ_{Bn}= 40°; 54% for θ_{Bn}= 50°; 42% for θ_{Bn}= 55°; 21% for θ_{Bn}= 59°). Beyond 60°, the reflected fraction falls to zero. From these simple calculations, which ignore the electrostatic potential which should increase reflection, we conclude that the observed upstream ions have most likely reflected from the shock. The excitation of magnetosonic waves by reflected ions was predicted by *Barnes* [1970]; such waves observed upstream of the earth's bow shock have been studied extensively [see e.g., *Lee*, 1982 and references therein].

To check that the large amplitude wave in Case 4 is caused by the pick-up ions, a case (Case 5) was run with the same parameters as Case 4 (Figure 4) except with no pick-up ions. Results for Case 5 for B_y, B_z, solar wind ion density and phase space are shown in Figure 5 at $t\omega_{ci}$ = 80. No long wavelength, large amplitude mode is present as was seen in Figure 4, thus verifying that the mode seen in Case 4 was caused by the upstream pick-up ions. In Figure 5, a few solar wind ions are seen upstream.

To examine the large amplitude magnetosonic waves of Case 4 (Figure 4) more closely, the total magnetic field B/B_0 for three time intervals near $t\omega_{ci}$ = 60 separated by a

time interval of 1 ω_{ci}^{-1} are plotted in Figure 6. From the figure, as well as from animation of the plots, it can be seen that the waves are moving towards the shock front. In the solar wind frame, the waves are propagating back upstream, as evidence by the steepening of the left (upstream) side of the wave packet. The shocklets move to the right because of convection by the solar wind. These large amplitude precursors are of interest because, they may lead to further energization of the pick-up ions via a first order Fermi acceleration process.

Simulations were performed for a range of angles (θ_{Bn}= 40–60°) and for M_A = 5 and 8. Figure 7 (Case 6) shows the waves excited for a simulation with the same parameters as in Case 4, but with a higher Mach number, M_A=8. Plotted at $t\omega_{ci}$ = 80 are B_y, B_z, the phase angle ϕ between B_y and B_z, solar wind and pick-up ion densities, and pick-up ion v_x-x phase space. Large amplitude magnetosonic waves excited by reflected pick-up ions are again present and two steepened shocklets are visible just ahead of the shock front. The amplitude here is still large ($\delta B_y/B_0 \approx 15\%$), although the waves appear smaller in this case because of the larger jump in the field at the shock (note the scale change on the magnetic field plots). The phase space shows that a large fraction of the pick-up ions have been reflected by the shock.

The reflected pickup ions in the oblique shocks, if detected by a spacecraft, could provide advanced warning of an encounter with the termination shock. In the de Hoffman-Teller frame, ions are specularly reflected. In the solar wind frame, the reflected particles have been energized and move upstream with a velocity much greater than the solar wind speed. Such ions can be seen in the pick-up ion phase space plots in Figures 4b and 7. Even allowing for the normal fluctions in the interplanetary magnetic field, some of these ions can be expected to escape back upstream.

To test the sensitivity of the wave excitation process to the upstream β, a simulation was run with all parameters as in Case 6 ($\beta_i = 0.2$, $\beta_e = 0.5$), but with $\beta_i = \beta_e = 0.1$. The results for wave excitation were quantitatively the same as Case 6. The sensitivity of the wave excitation process as a function of angle was also studied, although in shorter simulation boxes and for shorter times. Cases with M_A= 8, $\beta_i = 0.2$, $\beta_e = 0.5$, and with $\theta_{Bn} = 40°$, 50° and 60° were compared. In all cases, backstreaming pick-up ions were observed ahead of the shock and upstream magnetosonic waves were observed. The wave amplitudes and wavelengths were comparable for $\theta_{Bn} = 40°$ and 50°; for $\theta_{Bn} = 60°$, the wave amplitude was smaller and the wavelength longer.

4. Discussion

In summary, one-dimensional hybrid simulations have shown that a 10%-20% population of energetic solar wind pick-up ions will effect the structure of the termination shock, at least for the Mach numbers assumed here ($M_A \geq 5$). The termination shock is expected to be close to perpendicular on the average because of the tight winding of the Parker spiral in the outer heliosphere. However, based on the measured azimuthal angle of the interplanetary field in the outer heliosphere, the angle between the shock normal and the magnetic field will frequently fall in the $\theta_{Bn} = 40^o$–60^o range. Moreover, the shock angle becomes smaller towards the heliospheric poles.

For nearly perpendicular shocks, we find that the pick-up ions lead to the formation of an extended foot in front of the shock ramp of length approximately the gyroradius of the energetic pick-up ions. A foot ahead of the shock cause by O^+ pick-up ions was also seen in the cometary shock simulations of *Omidi et al.* [1986] for certain velocity distributions of the pick-up ions. In the simulations, the temperature increase in the pick-up ions across the shock was approximately that expected from adiabatic heating; this modest increase relative to the much larger solar wind ion "temperature" increase is at least partially due to the fact that the incoming "thermal" velocity of the pick-up ions is already comparable to the upstream flow velocity. As the fraction of pick-up hydrogen increases, the amount of shock dissipation provided by the pick-up ions increases. However, even at 20% pick-up hydrogen, the solar wind ions provide most of the dissipation.

For smaller angle shocks, $\theta_{Bn} \leq 60^o$, some of the reflected pick-up ions escape back upstream, gaining considerable energy in the process. These energetic backstreaming pick-up ions, if detected by a Voyager or Pioneer spacecraft in the outer heliosphere, may provide advanced warning of a near encounter with the termination shock. These reflected backstreaming ions excite very large amplitude ($\delta By/B_0 \approx$ 10%-25%) magnetosonic waves which are swept back into the shock by the solar wind flow. The magnetosonic waves, which propagate upstream in the solar wind frame, are observed to steepen into shocklets as they are convected towards the shock. Such shocklets have been seen at the Earth's bow shock and at comets and have been extensively studied in the past (*Omidi and Winske*, 1990; *Lee*, 1987 and references therein).

The generation of the upstream waves for the smaller angle shocks is of great interest because these waves may lead to a further energization of the pick-up ions via a first order Fermi-acceleration process (see *e.g.*, *Lee*, 1982 and references therein). In the shock frame, particles which bounce back and forth between the converting shock and upstream waves experience a net gain in energy. Energetic pick-up ions which are trapped

between the converging shock and magnetosonic waves may be further energized to cosmic rays. In this way, the pick-up ions may provide a seed population for anomalous cosmic rays. Energization and acceleration of pick-up ions at the termination shock will be investigated in the future.

Acknowledgments. We would like to thank C. Kennel, M. Neugebauer, M. A. Lee and D. W. Forslund for several valuable conversations. This work was carried out at the Jet propulsion Laboratory, California Institute of Technology, under a contract with the National Aeronautics and Space Administration. The research was supported in part by NASA/Heliospheric physics and in part by NSF under Cooperative Agreement No. CCR-8809615. Computer time on the Delta Touchstone Parallel Supercomputer was provided by NASA.

References

Barnes, A., Theory of generation of bow-shock-associated hydromagnetic waves in the upstream interplanetary medium, *Cosmic Electrodyn., 1*, 90, 1970.

Fisk, L. A., The anomalous component, its variation with latitude and related aspects of modulation, in *The Sun and the Heliosphere in Three Dimensions*, ed. by R. G. Marsden, D. Ridel, Hingham, Mass., 1986.

Fisk, L. A., Kozlovsky, B., and Ramaty, R., *Astrophys. J. (Letters), 190,* L35, 1974.

Gloeckler, G., Geiss, J., Fisk, L., Galvin, A., Ipavich, F., Ogilivie, K., and Wilken, B., Detection of interstellar pick-up hydrogen in the solar system, (submitted for publication), 1992.

Holzer, T. E., Interaction of the solar wind with the neutral component of the interstellar gas, *J. Geophys. Res., 77,* 5407, 1972.

Jokipii, J. R., Acceleration of cosmic rays at the solar wind boundary, *Astrophys. J. , 152,* 1968.

Jokipii, J. R., Particle acceleration at a termination shock, 1, Application to the solar wind and the anomalous component, *J. Geophys. Res., 91,* 2929, 1986.

Jokipii, J. R., Constraints on the acceleration of anomalous cosmic rays, *Astrophys. J. (Letters), 393,* L341, 1992.

Lee, M. A., The solar wind termination shock and the heliosphere beyond, in *Proceedings of the Sixth International Solar Wind Conference, II,* ed. by V. J. Pizzo, T. E. Holzer, and D. G. Sime, NCAR/TN-306+Proc, 1987.

Lee, M. A., Coupled hydromagnetic wave excitation and ion acceleration upstream of the earth's bow shock, *J. Geophys. Res., 87,* 5063, 1982.

Leroy, M. M., Winske, D., Goodrich, C. C., Wu, C. S., and Papadopoulos, K., The structure of perpendicular bow shocks, *J. Geophys. Res., 87,* 5081, 1982.

Liewer, P. C., and Decyk, V. K., A general concurrent algorithm for plasma particle-in-cell codes, *J. Comput. Phys., 85,* 302, 1989.

Mobius, E., Klecker, B., Hovesadt, D. and Scholer, M., Interaction of Interstellar Pick-Up Ions with the Solar Wind, *Astrophys. & Space Sci., 144,* 487, 1988.

Mobius, E., Pick-up of interstellar neutrals by the solar wind, *Adv. Space Res., 6,* 199, 1986.

Mobius, E., Hovestadt, D., Klecker, B., Scholer, M., Gloeckler, G., Ipavich, F. M., Direct observation of HE^+ pick-up ions of interstellar origin in the solar wind, *Nature, 318,* 426, 1985.

Omidi, N., and Winske, D., Theory and simulation of cometary shocks, *Geophys. Monograph, 61,* 37, 1991.

Pesses, M., Jokippi, J. R., and Eichler, D., Cosmic ray drift, shock wave acceleration, and the anomalous component of cosmic rays, *Astrophys. J. Lett.*, 246, L85, 1981.

Omidi, N., and Winske, D., A kinetic study of solar wind mass loading and cometary bow shocks, *J. Geophys. Res., 92,* 13,409, 1987.

Omidi, N., Winske, D., and Wu, C. S., The effect of heavy ions on the formation and structure of cometary bow shocks, *Icarus 66,* 165, 1986.

Smith, E. J., (private communication), 1992.

Smith, E. J., Magnetic fields in the heliosphere, in *Physics of the Outer Heliosphere*, ed. by S. Grzedzielski and D. E. Page, COSPAR, Pergamon, Oxford, 1990.

Vasyliunas, V. M., and Siscoe, G. L., On the flux and energy spectrum of interstellar ions in the solar system, *J. Geophys. Res., 81,* 1247, 1976.

Winske, D., and Leroy, M. M., Hybrid simulations techniques applied to the earth's bow shock, in *Computer Simulation of Space Plasmas--Selected Lectures at the First ISSS*, ed. by H. Matsumoto and T. Sato, D. Ridel, Hingham, Mass., 1985.

B. E. Goldstein and P. C. Liewer, Jet Propulsion Laboratory, California Institute of Technology, MS 169-506, 4800 Oak Grove Dr., Pasadena, CA 91109

N. Omidi, Department of Electrical and Computer Engineering, California Space Institute, University of California, San Diego, La Jolla, CA 92093

Figure Captions

Fig. 1. Histogram of the azimuthal angle θ of the interplanetary magnetic field at 35 AU using hourly averaged Pioneer 11 data. The distributions are centered approximately on perpendicular ($\pm 90^o$, depending on the sector) with a half width of about 25^o. Pioneer 11 was approximately 15^o out of the ecliptic [Courtesy of E. J. Smith].

Fig. 2. Simulation results for a quasi-perpendicular shock with 10% pick-up hydrogen, $\theta_{Bn}= 80^o$, $M_A = 8$, $\omega_{pi}/\omega_{ci}= c/V_A=7000$, $\beta_i= 0.2$, $\beta_e= 0.5$ and resistivity $\eta/4\pi=2 \times 10^{-5}/\omega_{pi}$(Case 1). (a) Plotted versus x ω_{pi}/c are magnetic field magnitude, total density n (normalized to the upstream value); solar wind (n_{sw}) and pick-up ion (n_p) densities (normalized to upstream values); and normalized solar wind and pick-up ion temperatures. Note the small foot extending ahead of the main shock ramp caused by backstreaming pick-up ions; the rise in the pick-up ion density coincides with the ramp. (b) Ion phase space plots for solar wind (S-W), showing a gyrating-reflected beam, and H+ pick-up (Hpickups) ions, showing the pick-up ions in the foot.

Fig. 3. Simulation results for a quasi-perpendicular shock with 20% pick-up hydrogen ions (Case 2); other parameters are as in Case 1 (Figure 2). (a) Plotted versus x ω_{pi}/c are magnetic field magnitude, total density n ; solar wind (n_{sw}) and pick-up ion (n_p) densities; and solar wind and pick-up ion temperatures, all normalized as in Figure 1. The foot ahead of the ramp, caused by backstreaming pick-up ions, is larger for this case with higher pick-up ion density. (b) Ion phase space plots for solar wind (S-W) and H^+ pick-up (Hpickups) ions. There is evidence of a gyrating-reflected beam in the pick-up ion phase space.

Fig. 4. Simulation results for an oblique $\theta_{Bn}= 50^o$ shock with 10% pick-up H^+ ions; other parameters are $M_A = 5$, $\omega_{pi}/\omega_{ci}= c/V_A=7000$, $\beta_i= 0.2$, $\beta_e= 0.5$, and $\eta =0$ (Case 4). (a) Plotted versus x are B_y, B_z, the phase angle ϕ in degrees between B_y and B_z, and the total, solar wind and pickup ion densities, all normalized as in Figure 1. Note the compressional magnetosonic wave ahead of the shock which has been excited by reflected pick-up ions. (b) Solar wind and pick-up ion phase space. Note the many backstreaming pickup ions (ions with $v_x <0$).

Fig. 5. Simulation results for a oblique $\theta_{Bn}= 50^o$ shock with no pick-ions (Case 5) and other parameters as in Case 4 (Figure 4). Plotted versus x are B_y, B_z, the phase

angle ϕ in degrees between B_y and B_z, and the solar wind density and the solar wind ion phase space. No large amplitude magnetosonic wave is seen ahead of the shock.

Fig. 6. Magnetic field profiles for Case 4 (Figure 4) for three times separated by 1 ω_{ci}^{-1} showing the steepening of the large amplitude magnetosonic waves. The waves propagate upstream (to the left) in the solar wind frame and steepen on the upstream side, but are swept into the shock by the solar wind flow.

Fig. 7. Simulation results for an oblique $\theta_{Bn}= 50^o$ shock with $M_A = 8$ and other parameters as in Case 4 (Figure 4). Plotted versus x are B_y and B_z, the phase angle ϕ in degrees between B_y and B_z, and the solar wind and pickup ion densities and the pick-up ion v_x-x phase space, all normalized as in Figure 1. Again, large amplitude compressional magnetosonic waves excited by backstreaming pickup ions are visible in the magnetic field and solar wind density profiles. The pick-up ion phase space shows the large fraction of backstreaming pickup ions.

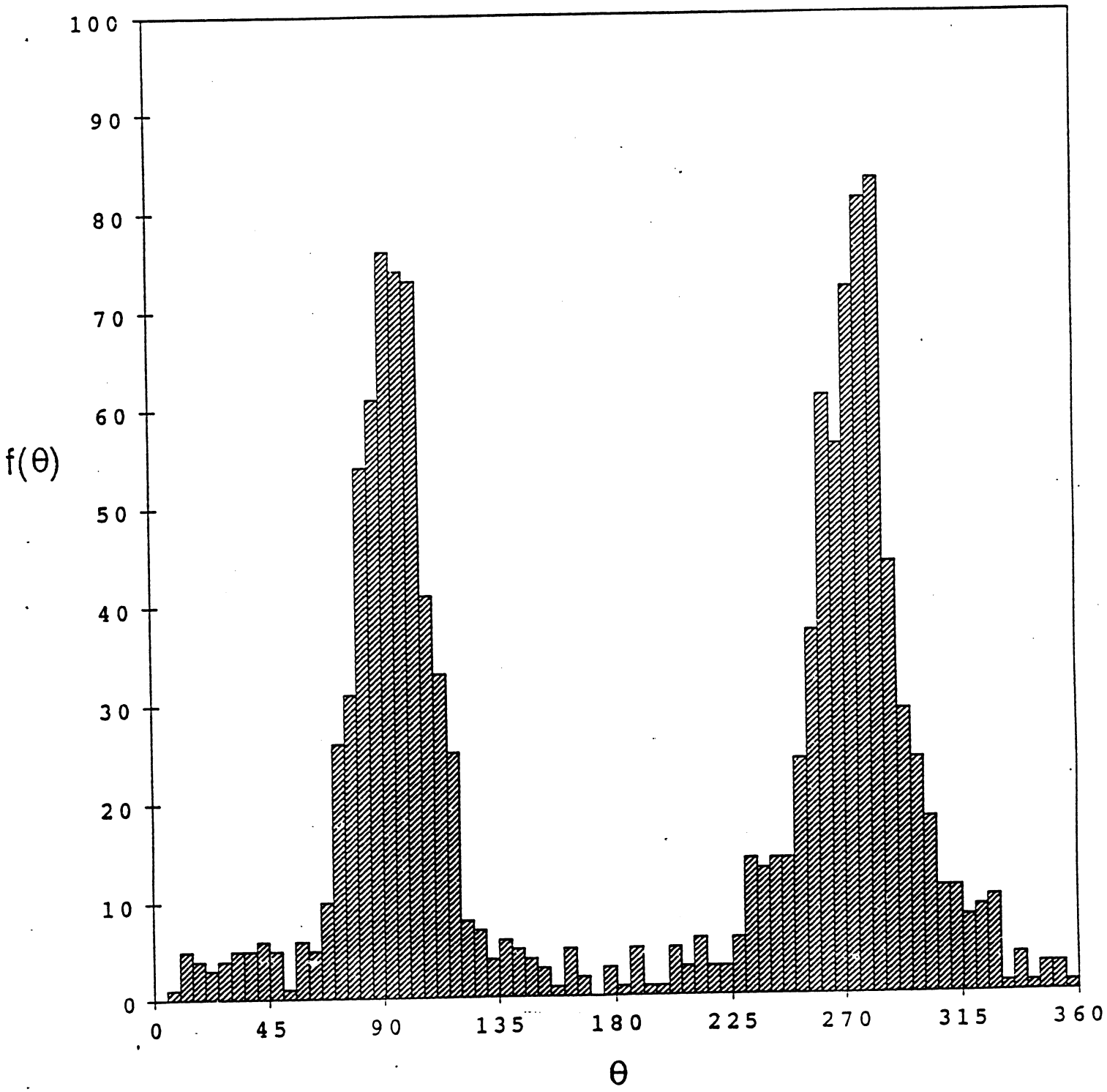

Fig. 1

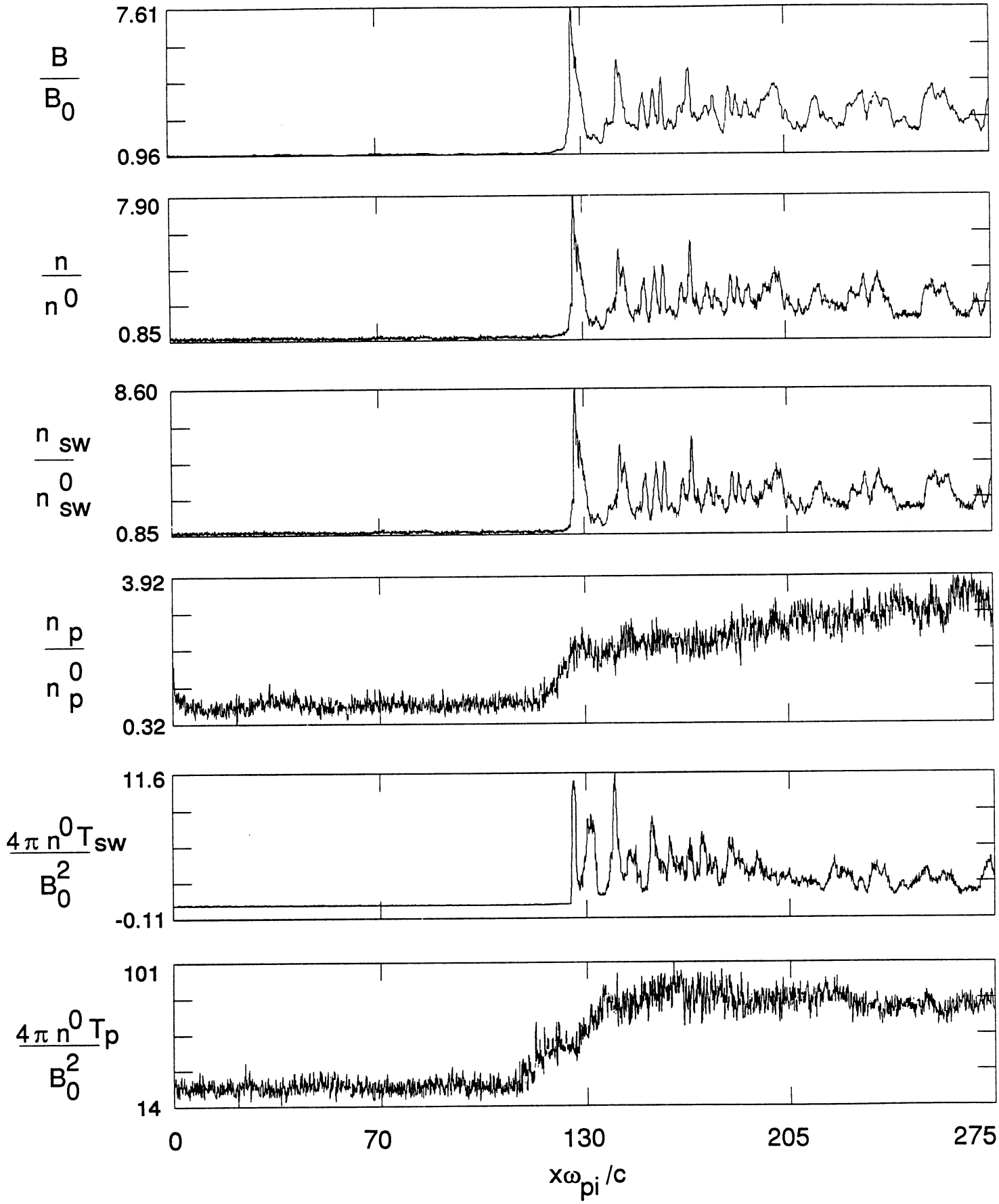
7.61
B/B0
0.96
7.90
n/n0
0.85
8.60
nsw/nsw0
0.85
3.92
np/np0
0.32
11.6
4πn0Tsw/B0^2
-0.11
101
4πn0Tp/B0^2
14
0
70
130
205
275
xωpi/c

Fig. 2a

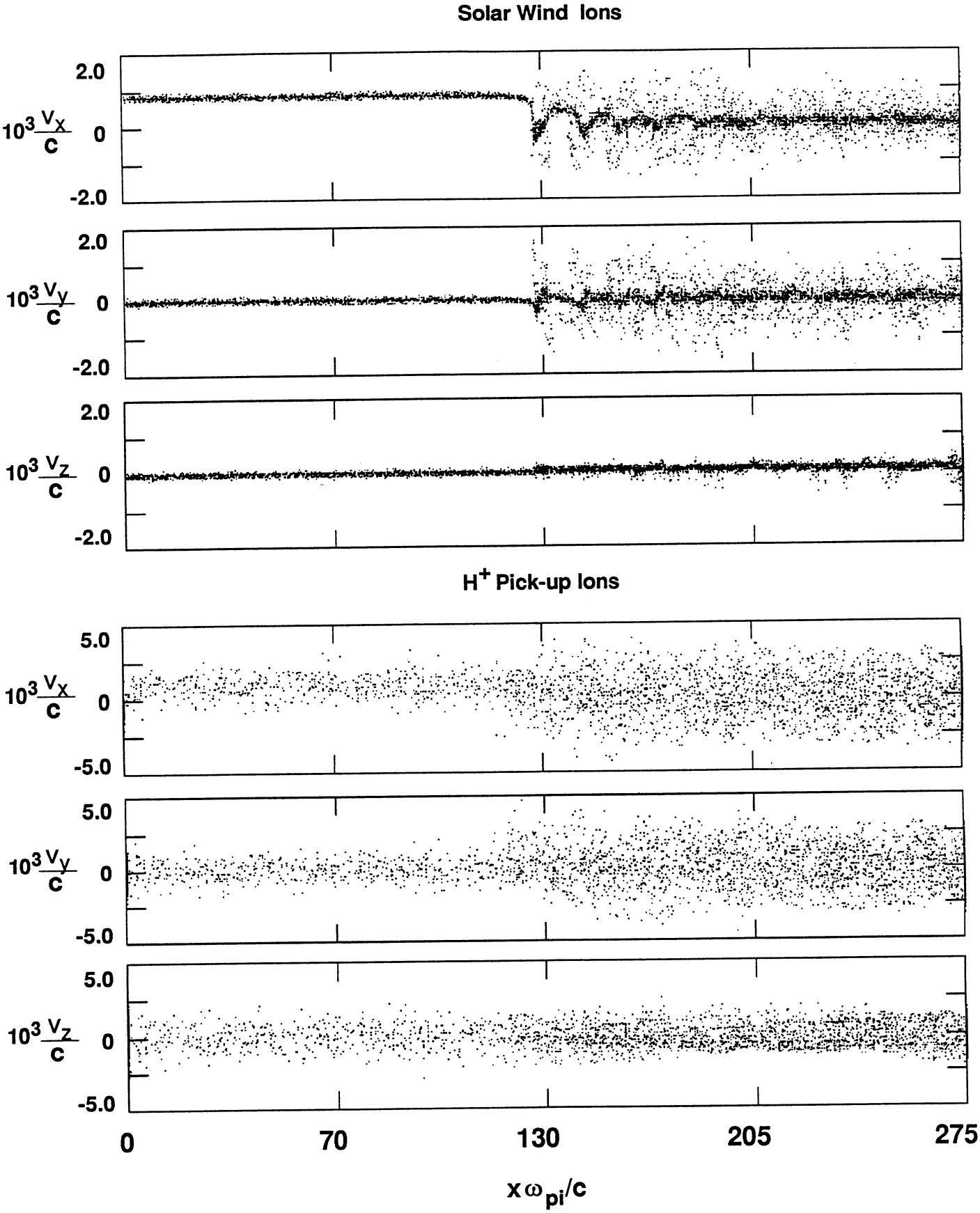
Solar Wind Ions
2.0
$10^3 \frac{V_x}{c}$ 0
-2.0
2.0
$10^3 \frac{V_y}{c}$ 0
-2.0
2.0
$10^3 \frac{V_z}{c}$ 0
-2.0
H^+ Pick-up Ions
5.0
$10^3 \frac{V_x}{c}$ 0
-5.0
5.0
$10^3 \frac{V_y}{c}$ 0
-5.0
5.0
$10^3 \frac{V_z}{c}$ 0
-5.0
0
70
130
205
275
$x\,\omega_{pi}/c$

Fig. 2b

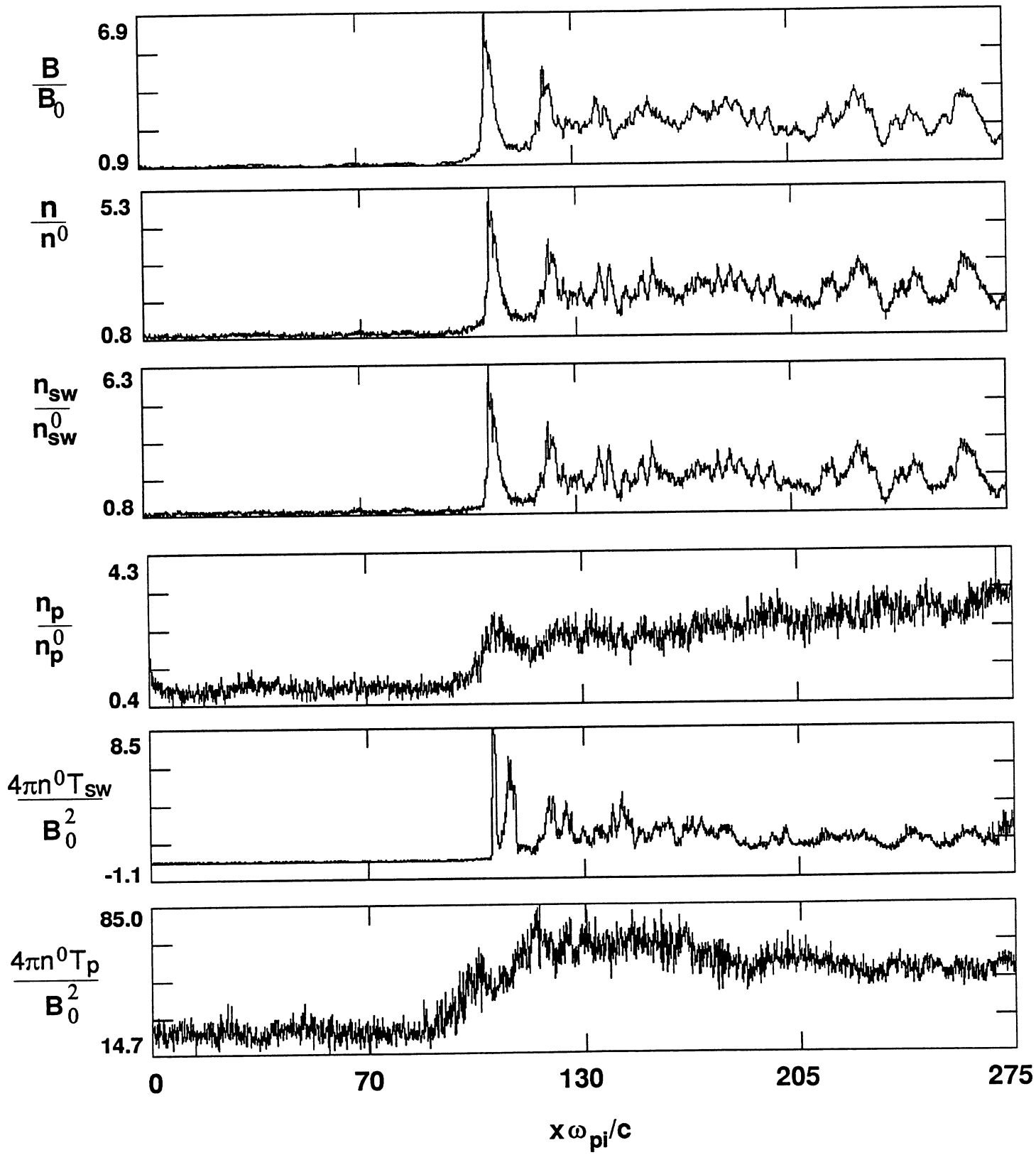
B/B0
6.9
0.9
n/n0
5.3
0.8
nsw/nsw0
6.3
0.8
np/np0
4.3
0.4
4πn0Tsw/B02
8.5
-1.1
4πn0Tp/B02
85.0
14.7
0
70
130
205
275
x ωpi/c

Fig. 3a

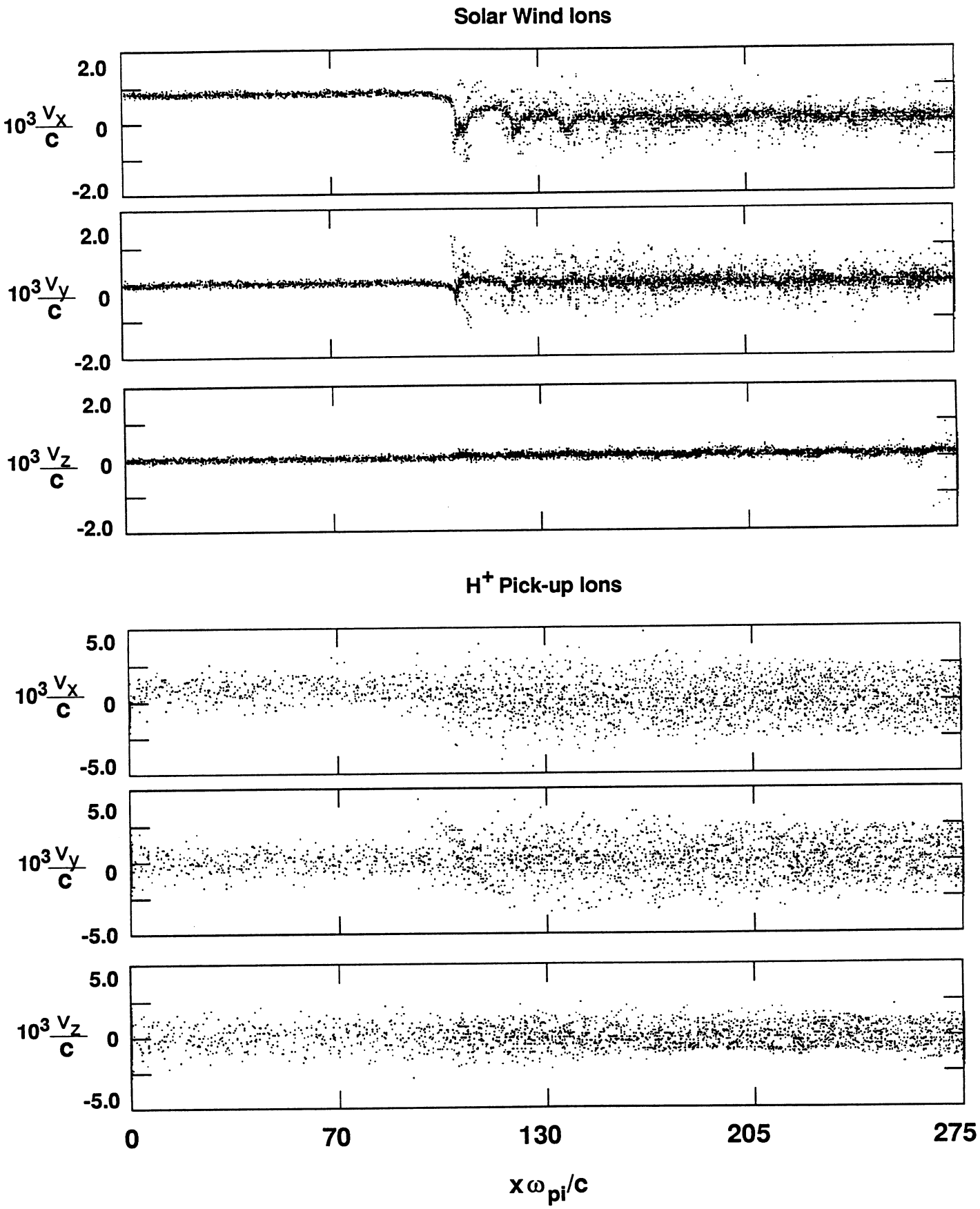
Solar Wind Ions
2.0
$10^3 \frac{v_x}{c}$
0
-2.0
2.0
$10^3 \frac{v_y}{c}$
0
-2.0
2.0
$10^3 \frac{v_z}{c}$
0
-2.0
H^+ Pick-up Ions
5.0
$10^3 \frac{v_x}{c}$
0
-5.0
5.0
$10^3 \frac{v_y}{c}$
0
-5.0
5.0
$10^3 \frac{v_z}{c}$
0
-5.0
0
70
130
205
275
$x\,\omega_{pi}/c$

Fig. 3b

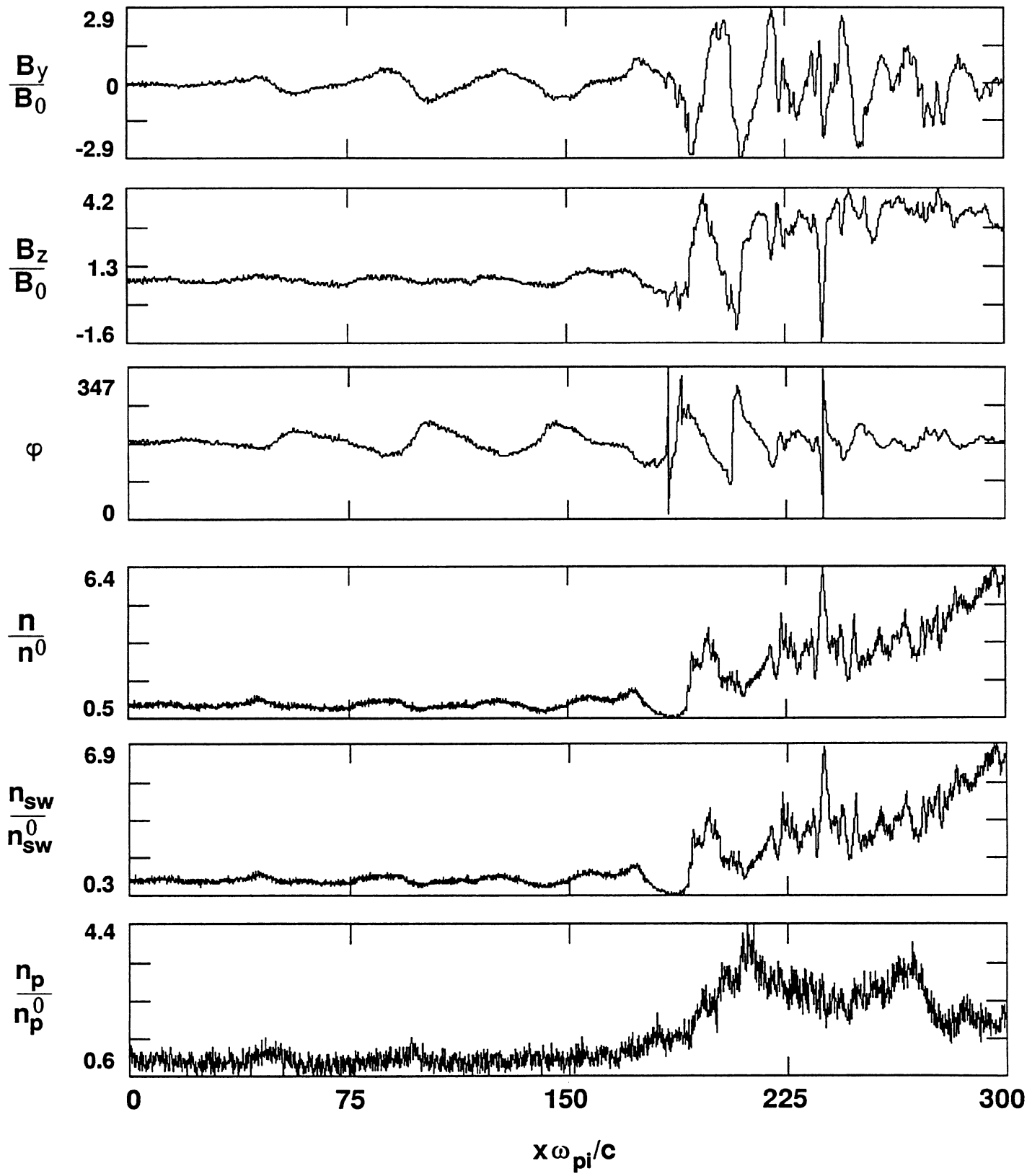
$\frac{B_y}{B_0}$
2.9
0
-2.9
$\frac{B_z}{B_0}$
4.2
1.3
-1.6
φ
347
0
$\frac{n}{n^0}$
6.4
0.5
$\frac{n_{sw}}{n_{sw}^0}$
6.9
0.3
$\frac{n_p}{n_p^0}$
4.4
0.6
0
75
150
225
300
$x\,\omega_{pi}/c$

Fig. 4a

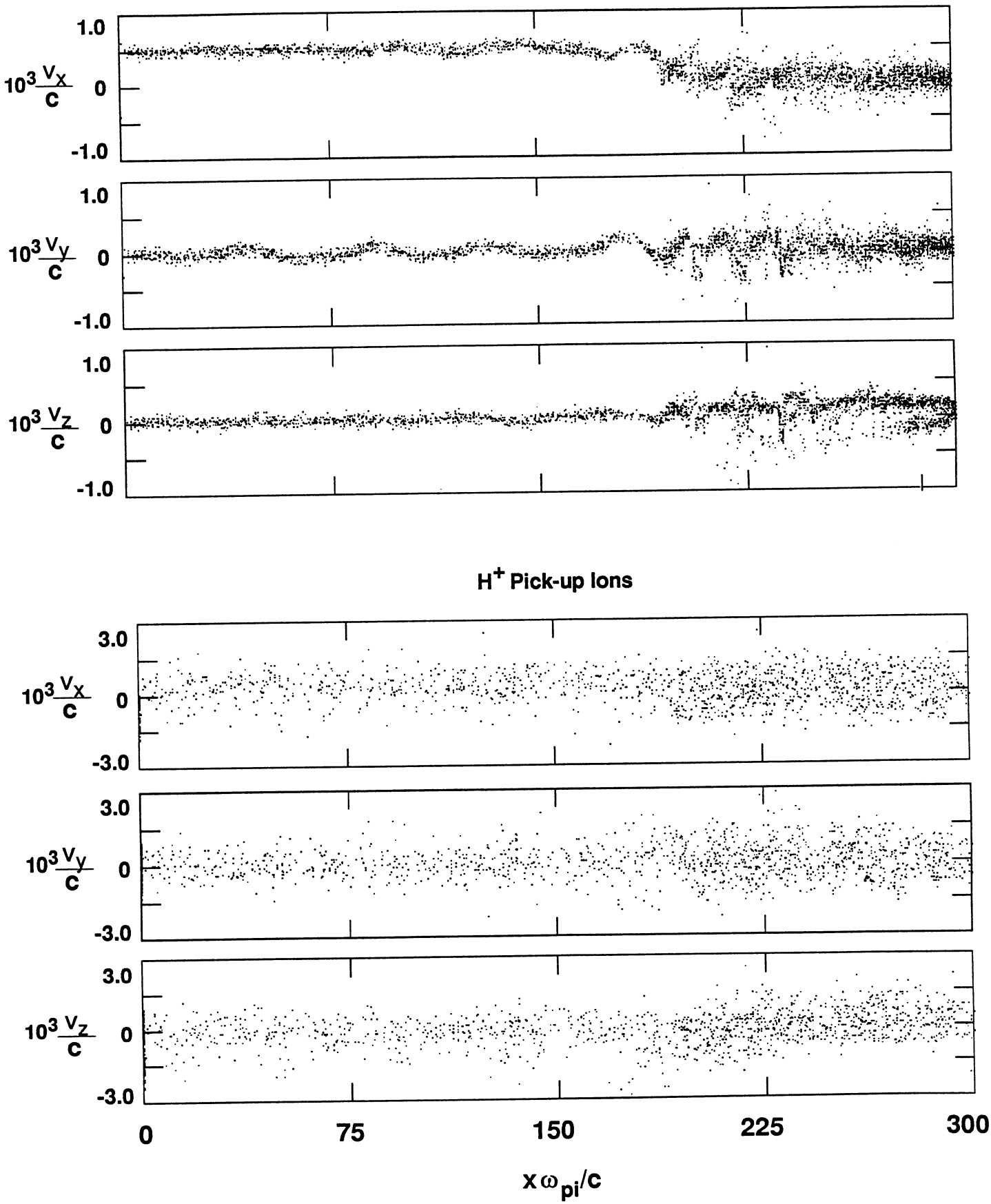
Solar Wind Ions
1.0
$10^3 \frac{V_x}{c}$
0
-1.0
1.0
$10^3 \frac{V_y}{c}$
0
-1.0
1.0
$10^3 \frac{V_z}{c}$
0
-1.0
H^+ Pick-up Ions
3.0
$10^3 \frac{V_x}{c}$
0
-3.0
3.0
$10^3 \frac{V_y}{c}$
0
-3.0
3.0
$10^3 \frac{V_z}{c}$
0
-3.0
0
75
150
225
300
$x\,\omega_{pi}/c$

Fig. 4b

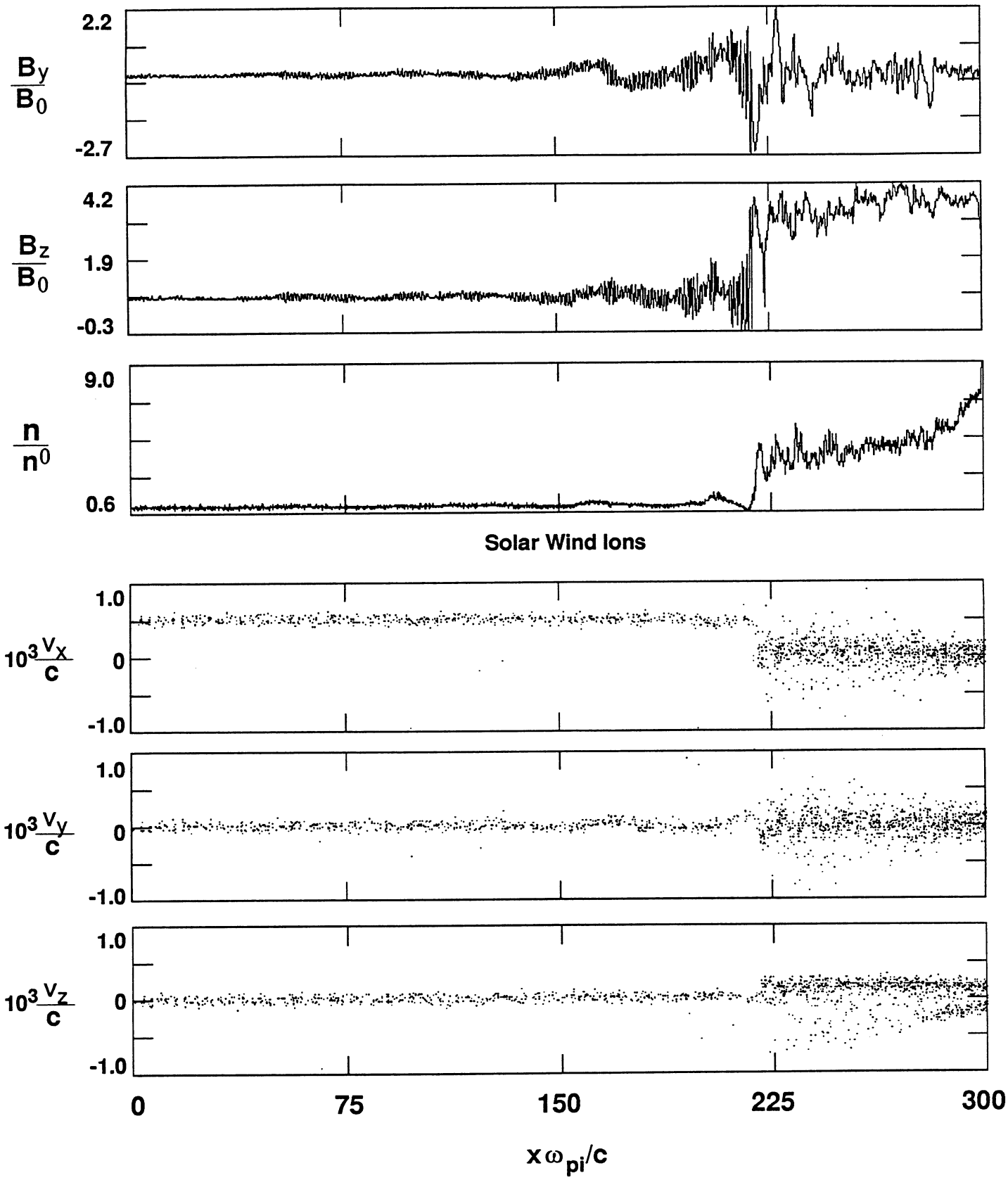
2.2
$\frac{B_y}{B_0}$
-2.7
4.2
$\frac{B_z}{B_0}$
1.9
-0.3
9.0
$\frac{n}{n^0}$
0.6
Solar Wind Ions
1.0
$10^3\frac{v_x}{c}$
0
-1.0
1.0
$10^3\frac{v_y}{c}$
0
-1.0
1.0
$10^3\frac{v_z}{c}$
0
-1.0
0
75
150
225
300
$x\,\omega_{pi}/c$

Fig. 5

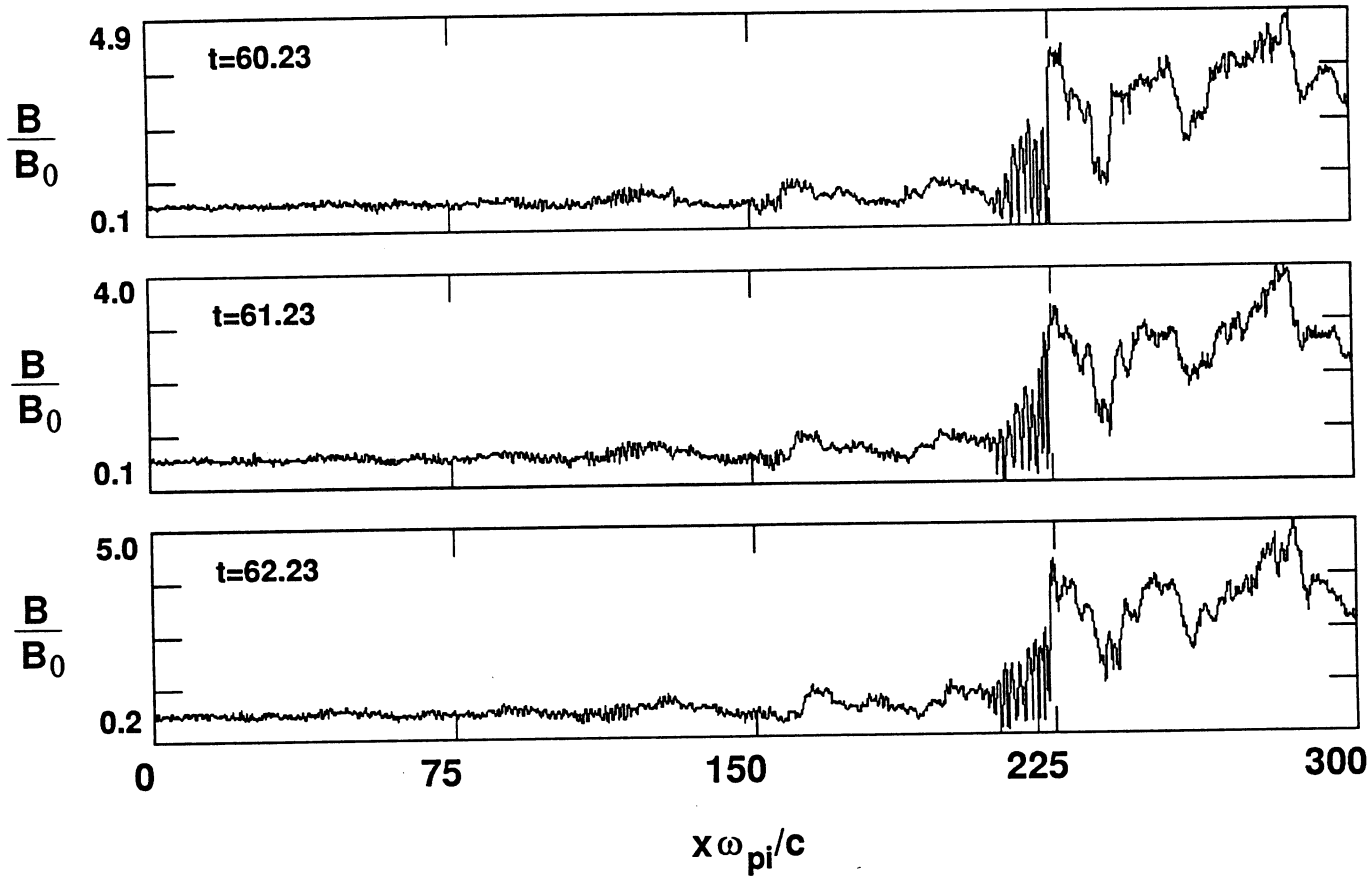
4.9
t=60.23
B/B0
0.1
4.0
t=61.23
B/B0
0.1
5.0
t=62.23
B/B0
0.2
0
75
150
225
300
x ωpi/c

Fig. 6

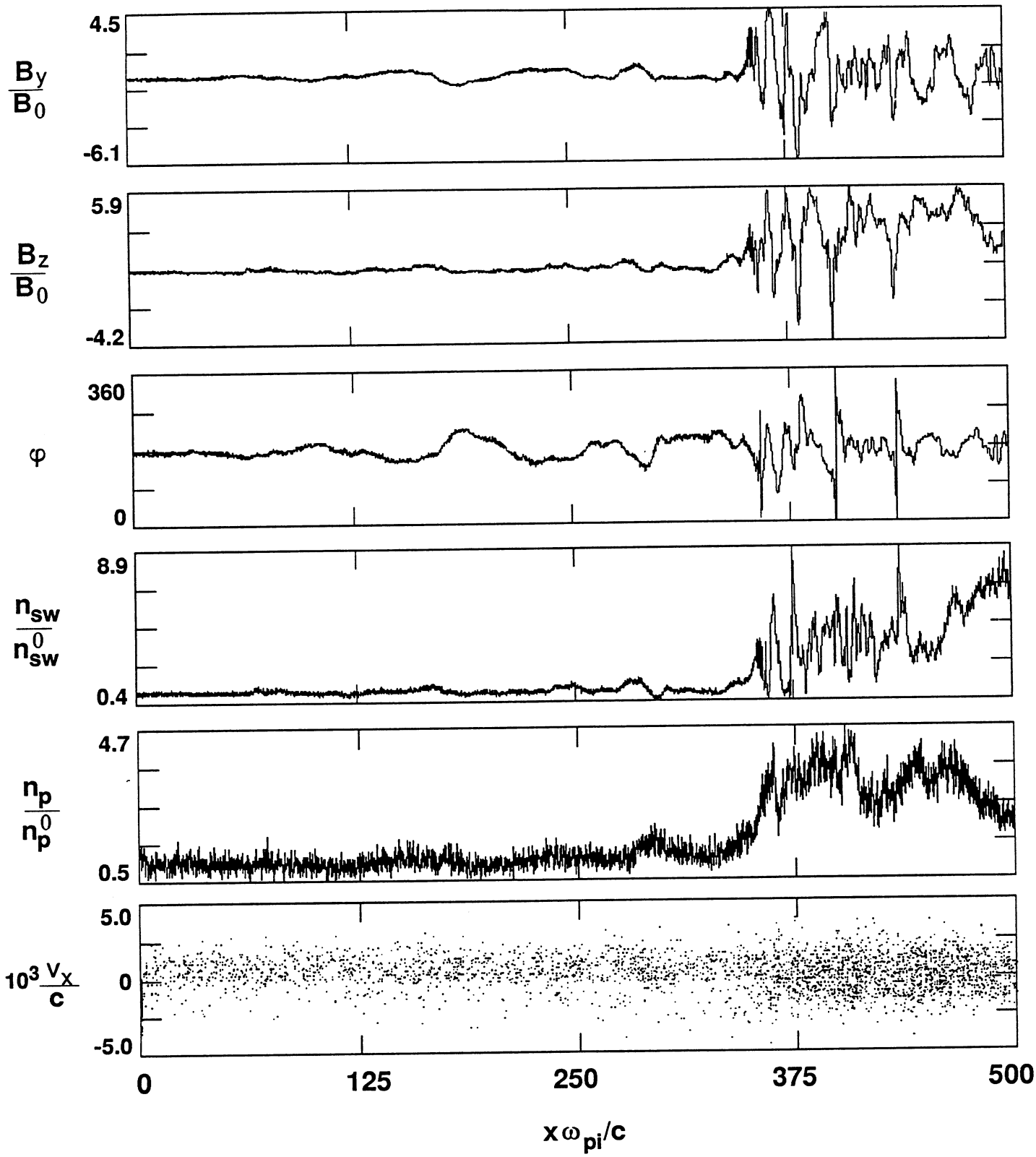
4.5
$\frac{B_y}{B_0}$
-6.1
5.9
$\frac{B_z}{B_0}$
-4.2
360
φ
0
8.9
$\frac{n_{sw}}{n_{sw}^0}$
0.4
4.7
$\frac{n_p}{n_p^0}$
0.5
5.0
$10^3 \frac{v_x}{c}$
0
-5.0
0
125
250
375
500
$x\,\omega_{pi}/c$

Fig. 7